







Comparing wire-mesh sensor with neutron radiography for measurement of liquid fraction in foam

M Ziauddin^{1,*} , E Schleicher², P Trtik³, L Knüpfer² , A Skrypnik¹ , T Lappan² , K Eckert^{1,2}  and S Heitkam^{1,2,*} 

¹ Technische Universität Dresden, Institute of Process Engineering and Environmental Technology, 01062 Dresden, Germany

² Helmholtz-Zentrum Dresden-Rossendorf, Institute of Fluid Dynamics, 01328 Dresden, Germany

³ Paul Scherrer Institut, Laboratory for Neutron Scattering and Imaging, 5232 Villigen PSI, Switzerland

E-mail: muhammad.ziauddin@tu-dresden.de and sascha.heitkam@tu-dresden.de

Received 6 September 2022, revised 12 October 2022

Accepted for publication 24 October 2022

Published 8 November 2022



Abstract

The liquid fraction of foam is an important quantity in engineering process control and essential to interpret foam rheology. Established measurement tools for the liquid fraction of foam, such as optical measurement or radiography techniques as well as weighing the foam, are mostly laboratory-based, whereas conductivity-based measurements are limited to the global measurement without detailed spatial information of liquid fraction. In this work, which combines both types of measurement techniques, the conductivity-based wire-mesh sensor is compared with neutron radiography. We found a linear dependency between the liquid fraction of the foam and the wire-mesh readings with a statistical deviation less than 15%. However, the wire-mesh sensor systematically overestimates the liquid fraction, which we attribute to liquid bridge formation between the wires.

Keywords: liquid fraction, foam, wire-mesh sensor, neutron radiography

(Some figures may appear in colour only in the online journal)

1. Introduction

In many industrial processes foam and froth play an important role. In some processes such as mineral flotation, froth is a key ingredient. In other processes like waste water recycling or beverage production, foam and froth constitutes a major risk for process failure [1]. The stability and mechanical behavior of the foam significantly depends on its liquid fraction ϕ . The liquid fraction is defined by the ratio of liquid volume to

total volume of a foam. Higher liquid fractions increase the stability of a foam by reducing the film rupture rate. On the other hand, high liquid fractions reduce the yield stress of a foam [2, 3] allowing the foam more easily to be removed by flushing with liquid. Consequently, the in-situ measurement of the liquid fraction of foam and froth in industrial devices would allow for better process control.

An established measurement tool for gas–liquid multi-phase flow measurement is the wire-mesh sensor (WMS) [4]. It has been used in research as well as in industrial applications [5]. While WMSs are well established for bubbly flows at high or medium liquid fraction [6], the application to flowing foam with low liquid fraction needs to be researched in more detail.

WMS can be based on both electrical conductance and capacitance [7]. However, within the scope of our experiment,

* Authors to whom any correspondence should be addressed.



Original Content from this work may be used under the terms of the [Creative Commons Attribution 4.0 licence](https://creativecommons.org/licenses/by/4.0/). Any further distribution of this work must maintain attribution to the author(s) and the title of the work, journal citation and DOI.

only the conductivity-based sensor is investigated. In WMS, two rows of wires are placed perpendicular to each other with a small spacing between the rows. An electric potential is applied to a transmitter wire. The corresponding current signal is received in another receiving wire and converted into a voltage U , yielding the local resistance at the crossing point of these two wires. There are several models available to calculate void fraction (opposite quantity of liquid fraction) of two-phase flow from local resistance, e.g. the Maxwell-Garnett model, the series model, or the parallel model [8]. In standard conductivity-based WMS, the void fraction (α) at a wire crossing is calculated from the sensor signal ($U^{\text{calibration}}$) for pure liquid (foaming solution in the case of foam) and the sensor signal for multiphase flow sample (U^{sample}) using the parallel mixing model

$$\alpha = 1 - \frac{U^{\text{sample}}}{U^{\text{calibration}}} \quad (1)$$

Thus, corresponding liquid fraction from the parallel model can be presented as follows

$$\phi = 1 - \alpha. \quad (2)$$

Feitosa *et al* presented an empirical relationship between the liquid fraction of foam and its relative conductivity (σ_{rel}) [9]

$$\phi = \frac{3\sigma_{\text{rel}}(1 + 11\sigma_{\text{rel}})}{1 + 25\sigma_{\text{rel}} + 10\sigma_{\text{rel}}^2}. \quad (3)$$

σ_{rel} can be derived from WMS signals as follows

$$\sigma_{\text{rel}} = \frac{U^{\text{sample}}}{U^{\text{calibration}}}. \quad (4)$$

In our experiment, we apply equations (3) and (4) to measure the liquid fraction of foam using WMS. Additionally, the liquid fraction of foam calculated using parallel model (equation (2)) will also be a part of this study.

To validate this approach, simultaneous neutron radiography (NR) measurements are applied. A beam of incoming neutrons is attenuated strongly by hydrogen which is present in the liquid phase of the foam [10]. For thermal neutrons, an equivalent thickness of 1 mm water attenuates 30% of the incoming neutrons. Therefore, the liquid fraction ϕ of aqueous foams, can be precisely measured in NR [11]. Previous work has proven that two-dimensional and instantaneous measurement of the liquid fraction with up to 10 fps and a spatial resolution below 1 mm is feasible using NR [10, 11].

2. Material and methods

2.1. Setup

Experiments were performed in a cylindrical foam column of 100 mm inner diameter and 550 mm height, made from acrylic glass and aluminum (figure 1(a)). The column was filled with 2 l of deionized water with 0.95 g l^{-1} sodium sulphate

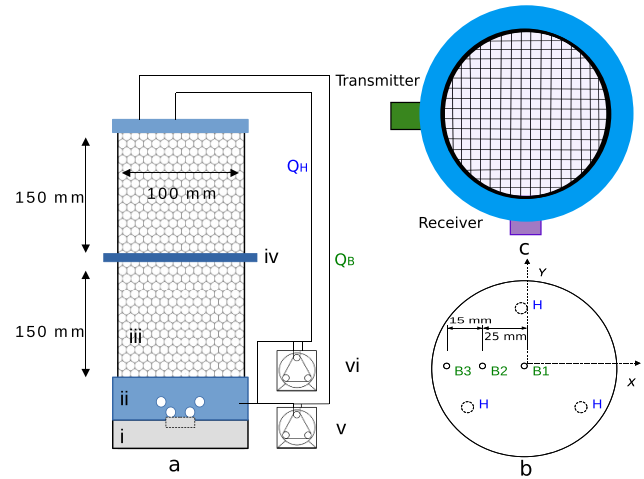


Figure 1. Foam cell setup; (a) front view: (i) foam generator, (ii) foaming solution, (iii) aluminum foam cell, (iv) DM100 WMS, (v) pump for in-homogeneity, (vi) pump for bulk flow; (b) top view: neutron beam direction indicated by Y and distance from center of the cell to the left and right denoted by X ; (H) bulk flow injection points (B) in-homogeneity injection points; (c) sketch of the 16×16 wires WMS.

(Na_2SO_4) and 6 g l^{-1} sodium dodecyl sulphate (SDS) solution, which is well above the critical micelle concentration (see table 1) and has viscosity of 0.9689 mPa s which is very close to the viscosity of pure water [12]. Bubbles were generated by applying an air flow of 1000 sccm to a bubble generator. Two different bubble generators were used, consisting of either 19 or 7 needles with an inner diameter of 0.6 mm and 1.2 mm, respectively. Air flow through the bubble generators produced bubbles of approximately 3 mm and 4.4 mm diameter, respectively.

A dynamic and a static case was investigated. Firstly, foam was produced continuously during the measurement. This resulted in a constant vertical foam velocity of 2.1 mm s^{-1} , computed from the gas flow rate. The steady foam flow resulted in a steady liquid fraction which was expected to be constant over the cross section of the WMS. Secondly, a static foam was produced by switching off the bubble production before measurement. For each run, the column was filled with fresh foam, displacing the old foam through the top opening. In this case, a forced drainage configuration was used [3]. A steady liquid flow Q is extracted from the reservoir below the foam by means of peristaltic pump (Ismatec MCP 404, Cole-Parmer GmbH) and added to the top of the foam column by means of 3 needles (denoted by H in figure 1(b)). In that way, a steady and homogeneous liquid fraction is established in the column, that can be controlled by the liquid flow Q . In addition, a steady but slightly inhomogeneous liquid fraction distribution can be imposed by feeding an additional liquid flow Q_2 by another peristaltic pump (Watson Marlow 120U, Watson Marlow Limited) to an additional needle. This additional needle can be mounted off-centered to one of the holes B1, B2 or B3 (figure 1(b)). This inhomogeneous liquid distribution may cause anisotropic drainage and thus, convective

instability [13]. Hence, simultaneous measurement of NR and WMS is required.

2.2. WMS

A WMS of 100 mm inner diameter with 16×16 stainless-steel wires of 0.5 mm diameter was used in the experiment. The distance between the adjacent wires is 6.25 mm which is called the pitch that defines the spatial resolution of the sensor, and the wire planes are 3 mm apart from each other. One set of wires consists of transmitting electrodes and another set of receiving electrodes. These two planes of wires are embedded in a cylindrical tube section of 100 mm inner diameter and made from the polymer FR4.

For each transmitter wire all receiver wires sense the electric current fully in parallel. The transmitter wires are activated sequentially one-by-one, applying a square wave excitation signal of 166.6 kHz. One complete frame of 16×16 wire crossings' is sampled within 0.1 ms, i.e. at 10 000 frames per second which enables measurement with 0.1 ms of temporal accuracy. A measurement of 10 s thus consists of $16 \times 16 \times 100\,000$ local instantaneous data points. For each experimental run data acquisition lasted for 10 s with subsequent temporal averaging over 100 000 frames to increase accuracy.

The WMS is sandwiched between two 3D-printed flange pieces of 20 mm height from polymer PLA, attached to aluminum sections of 150 mm height and 5 mm wall thickness.

For calibration, the WMS is submerged completely into a well defined solution of known conductivity (see table 1), yielding the conductance for 100% liquid fraction. In typical WMS applications, this calibration is performed with the identical liquid of the considered two-phase flow. However, the envisaged liquid fraction of the foam is in the order of 1% only. Consequently, the dynamic range between the electric currents in the calibration and in the foam measurement would be very high. Also, high amounts of Na_2SO_4 are added to the foaming solution in order to yield more precise measurements of the WMS. The resulting conductivity of the foaming solution equals 3.51 mS cm^{-1} . This might cause critically high currents in the calibration measurement, resulting in amplifier saturation. Therefore, a calibration solution with a significantly lower electric conductivity was employed (see tables 1 and 2).

Figure 2 shows the WMS reading σ_{WMS} against the conductivity of solutions containing varying concentrations of Na_2SO_4 , demonstrating the linear range for the conductivity of calibrating solution σ_{cl} ($610 \mu\text{S cm}^{-1}$), and for $176 \mu\text{S cm}^{-1}$ which is 0.05 times the conductivity of the foaming solution σ_{fl} (3.51 mS cm^{-1}), corresponding to foam at 5% liquid fraction.

The conductivity of the foaming solution σ_{fl} and of the calibration solution σ_{cl} was measured beforehand, using a conductivity meter (Five Easy Plus, Mettler Toledo, accuracy $\pm 2 \mu\text{S cm}^{-1}$). For foam measurement, the respective relative conductance was then converted to relative conductivity with respect to the foaming solution by a factor R . The liquid fraction of the foam was calculated using this relative conductivity σ_{rel} from equation (3)

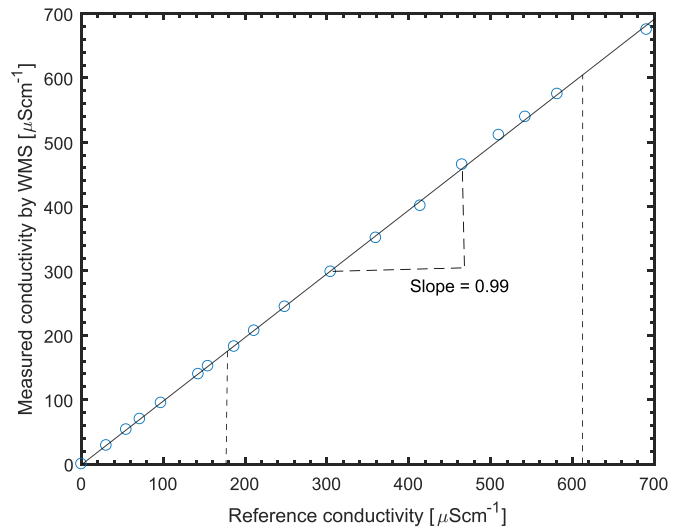


Figure 2. WMS measurements of the conductivity of Na_2SO_4 solutions with known conductivity.

Table 1. Foaming solution.

Surfactant (SDS)	6 g l^{-1}
Na_2SO_4	0.95 g l^{-1}
Deionized Water (H_2O)	21
Conductivity of Foaming Solution, σ_{fl}	3.51 mS cm^{-1}

Table 2. Calibrating solution.

Na_2SO_4	0.1 g l^{-1}
Deionized Water (H_2O)	51
Calibrating Solution Conductivity, σ_{cl}	0.61 mS cm^{-1}

$$R = \frac{\sigma_{\text{cl}}}{\sigma_{\text{fl}}} \quad (5)$$

$$\sigma_{\text{rel}} = \frac{\sigma_{\text{WMS}}}{R}. \quad (6)$$

Here, σ_{WMS} is the relative conductance returned from the WMS (equation (4)).

To avoid inhomogeneity due to wall effects, wire crossings within a distance of 5 mm to the wall are excluded from the further calculations (figure 3). The two-dimensional liquid fraction distributions are averaged along the diagonal direction (see figure 3) in order to represent the radiographic measurements. Each diagonal in figure 3 combines several WMS crossing points and yielded one data point in figures 7 and 8, below.

2.3. NR

NR is used to determine the two-dimensional distribution of the liquid fraction within the foam, integrated along the neutron beam direction.

A scintillator (LiF/ZnS , $200 \mu\text{m}$ thickness) converts the transmitted thermal neutrons into light which was detected and recorded by a CCD camera with $1024 \times 1024 \text{ px}$ and 1 s

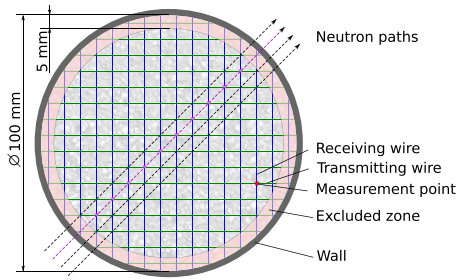


Figure 3. Schematic of 16×16 wires circular WMS inside of the frame. Border bound crossings, indicated by the red-shaded area, are excluded from the ϕ calculation. Direction of the neutron beams is shown by the arrow-lines, wire crossings are averaged diagonally along those lines for the liquid fraction calculation.

exposure time. The field of view was $125 \times 125 \text{ mm}^2$, yielding a spatial resolution of $122 \mu\text{m px}^{-1}$.

NR is strongly affected by the false detection of scattered neutrons. This scattering effect can be measured and compensated for by quantifying the scattered intensity behind black bodies and interpolate it over the whole image. The array of black bodies is visible in figure 4 as 25 black dots on an aluminum frame [11, 14]. The following equation was applied to derive the averaged thickness of water along the beam axis T_y from the neutron radiographs [11]

$$e^{-\mu_f T_y} = \left(\frac{I_{\text{foam}} - I_{\text{dc}} - I_f^s}{I_{\text{bg}} - I_{\text{dc}} - I_{\text{bg}}^s} \right) \frac{D(I_{\text{bg}} - I_{\text{dc}} - I_{\text{bg}}^s)}{D(I_{\text{foam}} - I_{\text{dc}} - I_f^s)}. \quad (7)$$

Here,

T_y	Thickness of the water content of the foam cell in the y direction (cm) [11]
μ_f	Attenuation co-efficient of water for thermal neutrons (3.6 cm^{-1})
I_{foam}	Image intensity of the foam with the black-body frame installed in front of the cell
I_{bg}	Image intensity of the empty cell with black-body frame installed (background image)
I_{dc}	Image resulted from the dark current of the CCD camera
I_{bg}^s	Image representation of the background scattering
I_f^s	Image representation of the sample scattering
D	Normalizing operator to account for variations in the beam intensity

Figure 4 depicts the NR image analysis. Figure 4(a) shows the background image I_{bg} . A single frame neutron radiograph of foam after removing the effect of scattering and gamma noises, I_{foam} can be seen in figure 4(b) while figure 4(c) shows the corresponding time-averaged image. 4(d) shows T_y , the thickness of water in the foam cell calculated from (7). Then the T_y was averaged over 37 pixels in width and 10 pixels in height. The averaged liquid contents are plotted in figure 4(d). These averaged values were divided by the corresponding chord length $L(x)$ of the foam cylinder to get the local liquid fraction averaged over y

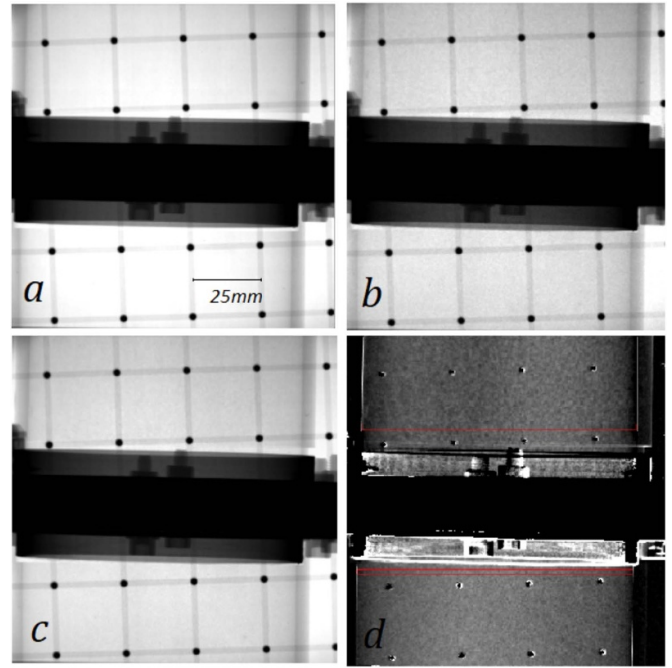


Figure 4. Processing neutron radiographs. (a) Background image, I_{bg} consisting of empty foam cell with back-bodies, (b) a single frame radiograph of foam filled cell, I_{foam} , (c) time-averaged radiograph of foam filled cell, I_{foam} , (d) liquid thickness of the foam projected in y -direction, T_y . ROI for the ϕ profile calculation is marked with red rectangles, above and below the WMS which is the dark region in the middle of the image.

$$L(x) = 2\sqrt{5^2 \text{cm}^2 - x^2} \quad (8)$$

$$\phi = \frac{T_y}{L(x)}. \quad (9)$$

The WMS probe itself is opaque to neutrons as its frame is made of acrylic material. Therefore, neutron imaging data were considered from the neutron transparent aluminum sections above and below the WMS sensor as marked in figure 4. An arithmetic average between the section above and below the WMS sensor gives the liquid fraction ϕ at the WMS position. The distribution of the liquid fraction ϕ was binned into 23 equidistant points to compare at identical ticks with WMS data, among which 21 points were considered in the comparison as sketched in figure 3.

A validation of the algorithm we used to calculate the liquid fraction of foam can be seen in the figure 5. Here a water filled thin wedge's water thickness was measured by NR, and the measurement has a deviation of less than 6% from the actual thickness.

3. Results

A typical measurement of spatial distribution of the liquid fraction ϕ from WMS using equation (3) is depicted in figure 6 from which we extract profiles of the liquid fraction. These WMS profiles (figure 7(b)) are compared to profiles obtained

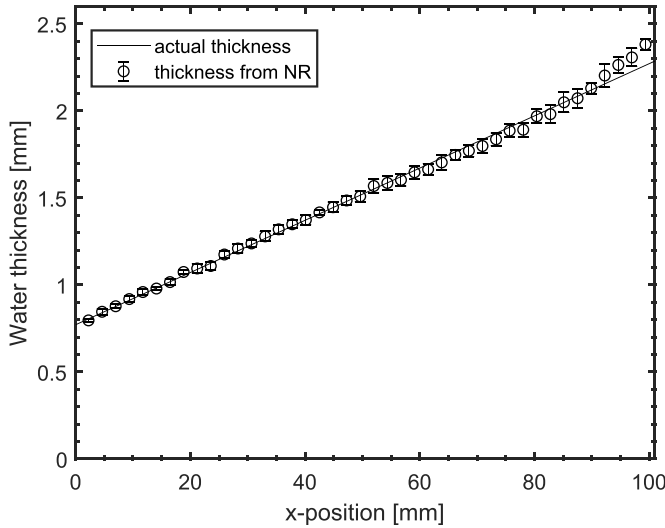


Figure 5. Measurement of the thickness of water of an wedge shaped cell filled with water by neutron radiography. The small circles indicate the measured thickness of the wedge and the error bars denote the standard deviation of the multiple measurements. Solid line shows the actual thickness of the wedge.

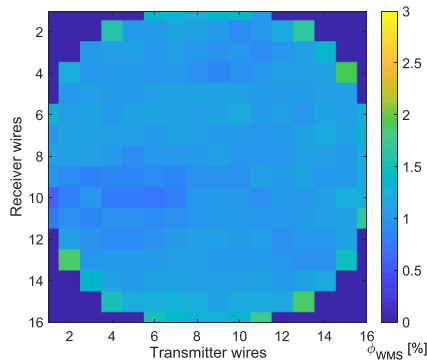


Figure 6. Two-dimensional distribution of the liquid fraction within the cell filled with fine foam of 3 mm bubbles. Homogeneous wetting (6 ml min^{-1}) is applied from the top of the cell.

from the NR measurements (figure 7(a)) for the case of 3 mm sized bubbles.

For the symmetric case without additional drainage flow and for the case with additional drainage flow through the center hole B1, a fairly homogeneous liquid fraction is measured. The slight increase in liquid fraction towards the right-hand side is reproduced by both measurements. In the case of additional drainage flow with medium (B2) and high (B3) inhomogeneity, a strong liquid fraction gradient occurs that is reproduced by both measurement techniques. Another profile for the flowing foam (7) also shows the similar reproduction in both measurements.

Figure 8 compares the liquid fraction profiles in case of bigger bubbles with 4.4 mm diameter. Generally, the profiles are similar to the smaller bubbles but show lower liquid fractions due to the lower drainage resistance than the finer foam [15].

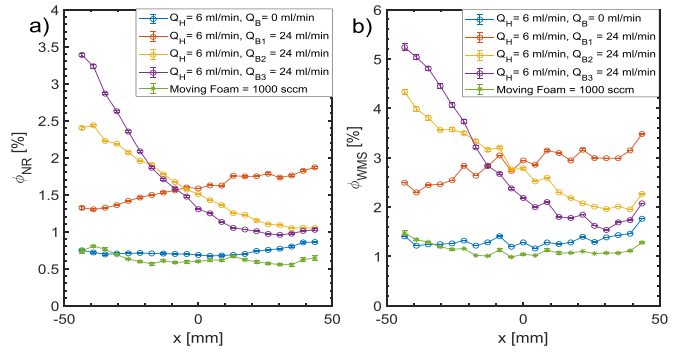


Figure 7. The liquid fraction profiles of the foam cell as a function of radial position (x coordinate), measured from the foam column's center in the projection plane for finer foam of 3 mm bubble diameter; (a) derived from NR, (b) derived from WMS. Mind the different scales of liquid fraction.

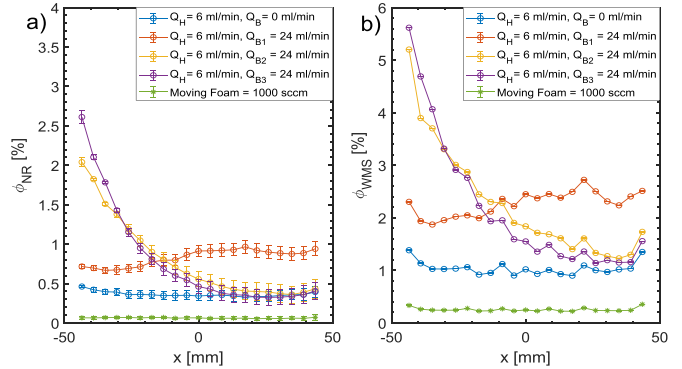


Figure 8. The liquid fraction profiles of the foam cell as a function of radial position (x coordinate), measured from the foam column's center in the projection plane for coarser foam of 4.4 mm bubble diameter; (a) derived from NR, (b) derived from WMS. Mind the different scales of liquid fraction.

The liquid fraction profiles are qualitatively reproduced by both measurement methods.

However, the liquid fraction is overestimated by WMS in a reproducible manner. To access the relation between WMS and NR measurements further, figure 9 compares all data points of figures 7 and 8, respectively.

Apparently, a clear, linear relation exists for smaller bubbles and larger bubbles at low liquid fractions. For larger bubbles at higher liquid fractions, the curve flattens. The standard deviation the measured data from this linear trend is less than 15% for small bubbles and less than 30% for large bubbles.

Another reproduction of liquid fraction measurement by WMS using parallel model can be seen in figure 10. It seems that liquid fraction measurement by WMS fits to the liquid fraction measurement by NR while simple parallel model (equation (2)) is used. However, the parallel model does not account for the liquid distribution in foam structure which can lead to the underestimation in the liquid fraction measurement of the finer foam (figure 10(a)).

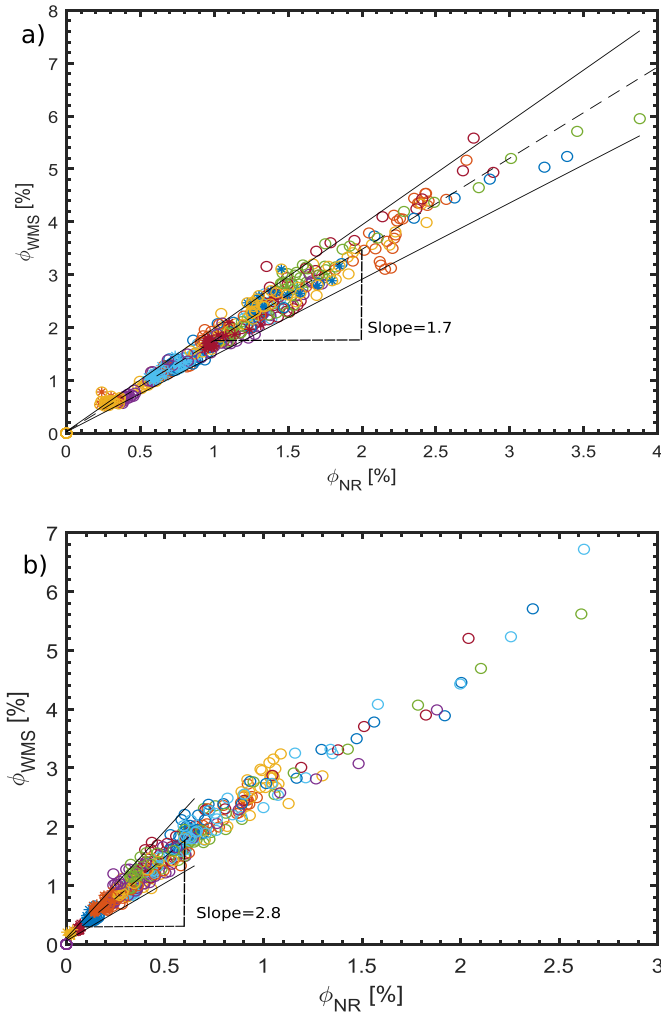


Figure 9. Liquid fraction ϕ_{WMS} as obtained by WMS using Feitosa model versus the liquid fraction ϕ_{NR} obtained by NR; (a) finer foam of 3 mm bubble diameter, (b) coarser foam of 4.4 mm bubble diameter. Static foam is marked by ‘o’ and moving foam is marked by ‘*’. Broken line is the linear approximation of the data and rigid lines are the deviation approximation of from the linearity.

4. Discussion

Liquid fraction profile in both measurement techniques shows quantitatively similar profiles for homogeneous and inhomogeneous wet foam irrespective of the bubble size.

However, the WMS overestimates the liquid fraction systematically by a factor between 1.7 and 2.8. Rechecking our measurement and computations very carefully, we are sure that this is not a failure in the data analysis or measurement uncertainty. The WMS operates well in its linear range (see figure 2). And also the measurement uncertainty of NR is significantly lower, as validation with a water wedge demonstrated (figure 5). Following Lorenceau *et al* [15], a drainage flow of 6 ml min^{-1} in our column of SDS foam would yield a liquid fraction of approximately 0.3% for larger bubbles (figure 8(a)) and 0.7% for smaller bubbles (figure 7(a)). This is in very good agreement with the NR data and underlines the systematic overestimation by the WMS sensor. The systematic

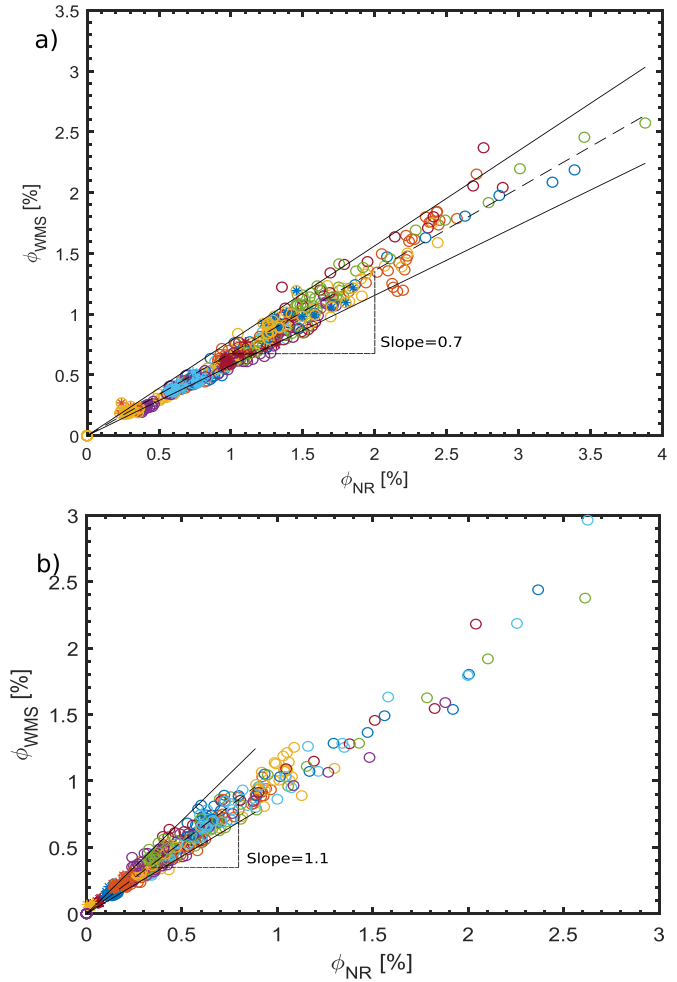


Figure 10. Liquid fraction ϕ_{WMS} as obtained by WMS using parallel model versus the liquid fraction ϕ_{NR} obtained by NR; (a) finer foam of 3 mm bubble diameter, (b) coarser foam of 4.4 mm bubble diameter. Static foam is marked by ‘o’ and moving foam is marked by ‘*’. Broken line is the linear approximation of the data and rigid lines are the deviation approximation of from the linearity.

overestimation results from the employed model for computing the liquid fraction ϕ from the relative conductivity σ_{rel} .

A similar effect is documented for WMS measurements in bubbly flow, where the liquid fraction is also overestimated [16, 17]. The model provided by Lorenceau *et al* [15] and also the Maxwell model do not represent the local topology of the foam structure between the wires. In order to identify a physically motivated model here more research regarding the local foam structure is required. Potentially, liquid bridges are formed between the crossing wires. These bridges could resemble similarities to Plateau borders. Following decoration theorem [18], the thickness of the bridging Plateau border would be in direct relation with the liquid fraction of the foam. It is evident from the slopes in figure 9, that bridging influences the WMS measurement stronger in the case of larger bubbles. This could be due to the fact, that the spacing between the wire planes equals 3 mm, which is similar to the size of the smaller bubbles, but much smaller than the size of larger bubbles. So potentially, a more stable bridge or Plateau border can be established at the wire crossings in case of larger

bubbles. For higher liquid fractions, the bridge becomes less dependent on the generally lower local capillary pressure in the coarser foam, yielding the saturation in figures 9 and 10. But these hypotheses need to be further investigated.

Previous work on liquid fraction measurement using parallel plate electrodes shows, when the liquid fraction measurement is carried out in larger distance to the foam liquid interface, it is less affected by capillary effects on liquid fractions [19]. In our experiment, measurements were made 100 mm above the foam-liquid interface which equals more than 50 times the capillary length of the foam. Consequently, our liquid fraction profile should not be influenced by capillary effects at the foam-liquid interface. Also, fringing electric field effects, common to parallel plate electrodes and depending on the distance between the electrodes, are negligible in WMS since the transmitter and receiver electrodes are placed very close (3 mm) to each other [20].

One disadvantage of WMS for foam measurement is the potential influence of the wires on the bubble size distribution due to film rupture or bubble cutting. However, comparing the liquid fraction above the WMS and below the WMS shows relative differences in temporally and spatially averaged liquid fractions below 15% in case of foam with homogeneous liquid fraction. Following the scaling law, which relates liquid fraction and mean bubble diameter of the foam for the given permeability [15], this corresponds to bubble size variations below 12%, which is negligible for many applications.

5. Conclusion

In-situ measurement of the liquid fraction of foam using WMS demonstrates the potential of WMS for the foam studies. The WMS allows to measure the spatial liquid fraction distribution with millimetric spatial resolution and at 10 kHz frame rate. The invasive nature of the measurement with wires causes a change in the mean radius of the bubbles which is less than 12% of the bubble radius. The WMS readings show a linear relation with the NR measurements of the liquid fraction for both fine and coarse foam. For larger bubbles at high liquid fractions, non-linear dependencies occurred. However, the measurement shows a systematic overestimation that needs to be quantified for different bubble sizes. Therefore, further studies are needed to investigate liquid bridge formation between receiving and transmitting electrodes for different bubble sizes and different distances between these two wire sets.

Data availability statement

The data that support the findings of this study are available upon reasonable request from the authors.

Acknowledgments

We thank Martin Tschofen (HZDR), Peggy Jähnigen (HZDR), Robin Michak (HZDR) and Jan Hovind (PSI) for their technical support in preparing and performing

these experiments. The financial support by the Deutsche Forschungsgemeinschaft (HE 7529/3-1), the German Federal Ministry for Economic Affairs and Energy (IGF Project No. 21151 BR), and the Bundesministerium für Bildung und Forschung (03HY123E) is gratefully acknowledged. This work is based on experiments performed at the Swiss spallation neutron source SINQ, Paul Scherrer Institute, Villigen, Switzerland.

Conflicts of interest

There are no conflicts to declare.

ORCID iDs

M Ziauddin  <https://orcid.org/0000-0002-4580-9482>
 L Knüpfer  <https://orcid.org/0000-0001-7012-7662>
 A Skrypnik  <https://orcid.org/0000-0002-3472-3421>
 T Lappan  <https://orcid.org/0000-0003-2826-1395>
 K Eckert  <https://orcid.org/0000-0002-9671-8628>
 S Heitkam  <https://orcid.org/0000-0002-2493-7629>

References

- [1] Morelle E, Rudolph A, McHardy C and Rauh C 2021 *Food Bioprocess Process.* **128** 63–76
- [2] Weaire D L and Hutzler S 2001 *The Physics of Foams* (Oxford: Oxford University Press)
- [3] Cantat I, Cohen-Addad S, Elias F, Graner F, Höhler R, Pitois O, Rouyer F and Saint-Jalmes A 2013 *Foams: Structure and Dynamics* (Oxford: Oxford University Press)
- [4] Prasser H-M, Böttger A and Zschau J 1998 *Flow Meas. Instrum.* **9** 111–9
- [5] Kipping R, Brito R, Scheicher E and Hampel U 2016 *Int. J. Multiph. Flow* **85** 86–95
- [6] Prasser H-M, Krepper E and Lucas D 2002 *Int. J. Therm. Sci.* **41** 17–28
- [7] Silva M J D, Schleicher E and Hampel U 2007 *Meas. Sci. Technol.* **18** 2245–51
- [8] Beyer M, Szalinski L, Schleicher E and Schunk C 2018 *Wire-Mesh Sensor Data Processing Software User Manual and Software Description, 2018* (Dresden: HZDR Innovation)
- [9] Feitosa K, Marze S, Saint-Jalmes A and Durian D J 2005 *J. Phys.: Condens. Matter* **17** 6301–5
- [10] Heitkam S, Rudolph M, Lappan T, Sarma M, Eckert S, Trtik P, Lehmann E, Vontobel P and Eckert K 2018 *Miner. Eng.* **119** 126–9
- [11] Carminati C et al 2019 *PLoS One* **14** e0210300
- [12] Kushner L M, Duncan B C and Hoffman J I 1952 *J. Res. Natl Bur. Stand.* **49** 85–89
- [13] Heitkam S and Eckert K 2021 *J. Fluid Mech.* **911** A54
- [14] Boillat P et al 2018 *Opt. Express* **26** 15769
- [15] Lorenceau E, Louvet N, Rouyer F and Pitois O 2009 *Eur. Phys. J. E* **28** 293–304
- [16] Prasser H-M, Misawa M and Tiseanu I 2005 *Flow Meas. Instrum.* **16** 73–83
- [17] Prasser H-M, Scholz D and Zippe C 2001 *Flow Meas. Instrum.* **12** 299–312
- [18] Weaire D 1999 *Phil. Mag. Lett.* **79** 491–5
- [19] Maestro A, Drenckhan W, Rio E and Höhler R 2013 *Soft Matter* **9** 2531
- [20] Hegg M and Mamishev A 2004 *Conf. Record of the 2004 IEEE Int. Symp. on Electrical Insulation* pp 384–7